Kalman Filter Cascade for Attitude Estimation on Rotating Earth

Joel Reis, Pedro Batista, Paulo Oliveira, and Carlos Silvestre

IEEE/ASME Transactions on Mechatronics, vol. 25, no. 1, pp. 327-338, February 2020

https://doi.org/10.1109/TMECH.2019.2959080

Kalman filter cascade for attitude estimation on rotating Earth

Joel Reis, Pedro Batista, *Senior Member, IEEE,* Paulo Oliveira, *Senior Member, IEEE,* and Carlos Silvestre, *Member, IEEE*

***Abstract*—This paper presents a discrete-time attitude estimation solution based on a cascade of two linear time-varying Kalman filters (KFs). Under mild assumptions, the cascade's first KF resorts to body-fixed measurements of angular velocity and of a constant inertial vector to yield an estimate of Earth's angular velocity. The latter, in addition to all previous measurements, is fed to the second KF to obtain an estimate of the rotation matrix. Although topological constructions are lifted, a last-step projection operator is employed that maps the final rotation matrix estimate onto $SO(3)$. Briefly, two linear time-varying systems are designed, with no linearisations whatsoever, that are shown to be uniformly completely observable, thus rendering the overall solution globally exponentially stable. Simulation results are presented that allow to assess the performance of the cascaded KF duo. A set of experimental results is also presented that validates the efficiency of the proposed solution and deems it a suitable attitude estimation choice for applications where only one body-vector measurement is available.**

***Index Terms*—Attitude Estimation, Kalman Filter, Earth Angular Velocity, High-Grade Rate Gyros, Uniform Complete Observability**

I. Introduction

DETERMINING the attitude of a body allows to describe how it is oriented in its enclosing space. Attitude measurements, often expressed by rotation matrices with respect to a known inertial reference frame, represent crucial information across important engineering fields, for instance, in control of earth-orbiting satellites and spacecrafts [1], [2], in navigation problems [3], [4], in mobile robot applications [5], [6], etc.

The Wahba's problem, one of the first approaches to the classic problem of satellite attitude estimation, proposed a means of determining the best least squares fit over two sets of observed points as to obtain a proper orthogonal matrix [7]. The purely algebraic solution to this problem does not include steps of noise removal and reduction, thus leaving the door open for the development of filters and observers capable of smoothing estimated data, based on the use of complementary information from a set of appropriate sensors.

J. Reis and C. Silvestre are with the Department of Electrical and Computer Engineering of the Faculty of Science and Technology, University of Macau, Taipa, Macao (e-mail: joelreis@um.edu.mo; csilvestre@um.edu.mo)

P. Batista and P. Oliveira are with the Institute for Systems and Robotics, Instituto Superior Técnico, Universidade de Lisboa, Lisboa 1049 001, Portugal (e-mail:pbatista@isr.tecnico.ulisboa.pt; paulo.j.oliveira@tecnico.ulisboa.pt)

P. Oliveira is also with LAETA—Associated Laboratory for Energy, Transports and Aeronautics, IDMEC—Institute of Mechanical Engineering, Instituto Superior Técnico, Universidade de Lisboa, Lisboa 1049-001, Portugal.

C. Silvestre is on leave from Instituto Superior Técnico, Universidade de Lisboa, Lisboa, Portugal.

Soon, the celebrated extended Kalman filter (EKF) became a frequent solution for nonlinear attitude estimation applied to a broad range of applications. Amid an extensive literature on the subject, see, e.g., the works in [8] and [9], which raised awareness for the pitfall associated with linearizations of propagation equations, and with model inaccuracies.

There have been, however, efforts to detour around these two major drawbacks. Particularly, in [10] an optimal linear attitude estimator is presented that applies the Cayley conformal mapping over the rotation matrix in order to build a linear unconstrained problem; and, the work in [11] proposes a discrete-time attitude observer, where no knowledge of the attitude dynamics model is assumed, based on a discretized Lagrangian inspired by Wahba's problem.

Nevertheless, despite its inherent limitations, the EKF remained a popular choice in terms of nonlinear estimators, and is still actively researched today. Recently, the work in [12] presented, in a deterministic context, a solution based on symmetry preserving observers and on the invariant EKF, which, under certain observability conditions, is shown to be an asymptotic observer. From the same authors, in [13] a class of simple filters is proposed, on Lie groups, whose discrete-time error's evolution is independent of the system's trajectory. In one of the problem settings illustrated therein, the rotation of the Earth is taken into account, an interesting practical scenario which is tackled in this paper.

Typically, in most mission layouts, the rotating body's angular velocity is available through gyro sensors. Thanks to recent advances in the development of high-grade rate gyroscopes, such as the commercial off-the-shelf fiber optic gyro (FOG) inertial measurement unit (IMU) KVH® 1775, the Earth's instantaneous rotation vector can also be perceived with precision, although not explicitly.

This fact motivated the previous work by the authors, presented in [14]–[16], where single body-fixed vector measurements of a constant inertial vector and of a triaxial high-grade rate gyro are considered. In [14], it is shown that with only implicit knowledge of the Earth's spin, it is still possible to design an attitude observer, but with extremely slow settling times (around 24 hours). In [15], a globally exponentially stable (GES) cascade observer explicitly estimates the Earth's angular velocity, and then estimates the rotation matrix without topological constraints. Alternatively, in [16] the estimates of the rotation matrix evolve on the 2-sphere manifold but without global stability guarantees. As opposed to those works, in this paper, the discrete-time Kalman filter cascade has faster convergence rates, and entails a much simpler and

straightforward tuning process through its covariance matrices, bypassing the need for piecewise gains. Furthermore, experimental results are presented that validate the efficiency of the proposed technique.

With explicit knowledge of two body-fixed vector measurements, it is always ensured, under a mild geometrical assumption between these vectors, that the attitude can be uniquely determined at every instant. Hence, estimating a second vectorial measurement when only one is available is of paramount importance. This has recently been addressed in the construction of a discrete attitude observer for fusing monocular vision with GPS velocity measurements [17], and was also studied in [2] to solve an attitude control problem by output feedback. In [18], an algorithm is proposed, focused on ground-based robots subjected to low body-accelerations, that uses accelerometer data and rate gyro sensors.

This work builds upon [15] by proposing a cascade of two discrete-time linear time-varying (DT-LTV) Kalman filters (KFs) for the problem of attitude estimation considering a full discrete-time setting, as opposed to systems with continuous-time models and discrete-time observations [13]. The objective behind the first filter is to estimate a second vector measurement, which, in this case, corresponds to the Earth's angular velocity. This estimate, combined with measurements of another body-fixed vector, will be used by the second filter to determine the rotation matrix. Most noticeably, there is no linearization involved in the design of the proposed cascade, as it stems from an exact discretization of the system dynamics proposed in [15]. Despite not evolving on $SO(3)$, the second KF's estimates are shown to converge globally exponentially fast to elements of this manifold, as the underlying linear system is proved to be uniformly completely observable (u.c.o).

This system can be used in scenarios where high-accuracy is a key demand, for instance, on ships and submarines as an alternative to gyrocompass-based solutions, or used for stabilization purposes concerning rotational platforms.

This paper is organized as follows: in Section II, a brief introduction of the problem statement and the design of the first KF to estimate the Earth's angular velocity are presented. In Section III, the construction of the cascade is completed with the design of the second KF, which yields an estimate of the rotation matrix. Both Sections II and III also feature, in a similar fashion, an extensive observability analysis. Section IV includes simulation results that allow to validate the performance of the KF cascade. In Section V, an experimental setup is described and its results reported, further allowing to assess the effectiveness of the proposed solution in real world applications. Finally, a summary of the main results of this paper is drawn in Section VI.

A. Notation

Throughout the paper, a bold symbol stands for a multi-dimensional variable, the symbol $\mathbf{0}$ denotes a matrix of zeros and $\mathbf{I}$ an identity matrix, both of appropriate dimensions. When suitable, $\mathbf{I}_n$ conceals an identity matrix of dimensions $n \times n$. A block diagonal matrix is represented as $\text{diag}(\mathbf{A}_1, \ldots, \mathbf{A}_n)$. The Special Orthogonal Group is denoted by $SO(3) := \{\mathbf{X} \in \mathbb{R}^{3\times 3} : \mathbf{X}\mathbf{X}^T = \mathbf{X}^T\mathbf{X} = \mathbf{I} \wedge \det(\mathbf{X}) = 1\}$. In $\mathbb{R}^3$, the skew-symmetric matrix of a vector $\mathbf{a} \in \mathbb{R}^3$ is defined as $\mathbf{S}(\mathbf{a})$, such that given another vector $\mathbf{b} \in \mathbb{R}^3$ one has $\mathbf{a} \times \mathbf{b} = \mathbf{S}(\mathbf{a})\mathbf{b}$. The Kronecker sum and product are represented by $\oplus$ and $\otimes$, respectively. $\mathcal{N}(\boldsymbol{\mu}, \boldsymbol{\sigma})$ stands for a multivariate normal distribution with mean $\boldsymbol{\mu}$ and standard deviation $\boldsymbol{\sigma}$. Finally, for convenience, the transpose operator is denoted by the superscript $(\cdot)^T$.

II. Estimation of Earth's Angular Velocity

This section provides the basis for the development of an attitude estimator. The problem statement is first explained, followed by the design of a KF to produce estimates of the Earth's angular velocity.

Suppose there is a robotic platform equipped with a tri-axial high-grade FOG IMU, e.g., the KVH® 1775, that provides angular velocity readings in addition to sensor-body measurements of a vector whose inertial counterpart is constant. In applications where the magnitude of the gravitational field dominates the value of the body's acceleration for low frequency response, one may assume that the inertial acceleration is a constant vector [19]. Furthermore, assume that the IMU's rate gyros are sensitive to the Earth's velocity of rotation. Hence, the first stage aims at computing an estimate of the angular velocity of the Earth as expressed on the body coordinate system installed on the robotic platform.

A. Continuous-time preface to the problem statement

Following in the steps described in [15], let $\mathbf{R}(t) \in SO(3)$ denote the rotation matrix from a body-fixed frame $\{B\}$ to a local inertial coordinate reference frame $\{I\}$[1]. The evolution in time of $\mathbf{R}(t)$ obeys

$$\dot{\mathbf{R}}(t) = \mathbf{R}(t)\mathbf{S}[\boldsymbol{\omega}(t)], \tag{1}$$

where $\boldsymbol{\omega}(t) \in \mathbb{R}^3$ is the angular velocity of $\{B\}$ with respect to $\{I\}$, expressed in $\{B\}$. The high-grade rate gyro measurements are given by $\boldsymbol{\omega}_m(t) = \boldsymbol{\omega}(t) + \boldsymbol{\omega}_E(t)$, where $\boldsymbol{\omega}_E(t) \in \mathbb{R}^3$ is the angular velocity of the Earth around its own axis, as expressed in $\{B\}$. In turn, let the single body-vector measurements be denoted as $\mathbf{m}(t) \in \mathbb{R}^3$. These, when expressed in inertial coordinates, are assumed constant. Let ${}^I\boldsymbol{\omega}_E$ and ${}^I\mathbf{m}$ be the inertial vector counterparts corresponding to $\boldsymbol{\omega}_E(t)$ and $\mathbf{m}(t)$, respectively, such that ${}^I\boldsymbol{\omega}_E = \mathbf{R}(t)\boldsymbol{\omega}_E(t)$ and ${}^I\mathbf{m} = \mathbf{R}(t)\mathbf{m}(t)$ for all $t \geq 0$. For ease of notation, the upper left superscripts of body vectors are dropped, i.e., $\boldsymbol{\omega}_E \equiv {}^B\boldsymbol{\omega}_E$ and $\mathbf{m} \equiv {}^B\mathbf{m}$.

As previously argued, prior to unequivocally computing an estimate of the rotation matrix, one needs to determine a second vector, in addition to the one measured, $\mathbf{m}(t)$. In order to do so, define as system states $\boldsymbol{x}_1(t) := \mathbf{m}(t)$ and $\boldsymbol{x}_2(t) := \boldsymbol{\omega}_E(t) \times \mathbf{m}(t)$. Notice that state $\boldsymbol{x}_2(t)$ closely relates to the Earth's angular velocity, and further notice that $\boldsymbol{x}_1(t)$, albeit known, will undergo a noise-filtering procedure. Finally,

[1]The frame $\{I\}$ is not exactly an inertial frame in the sense of the classical physics, but can be considered as such for this application because the apparent forces due to the Earth's movement are within the accelerometer's errors, which was the sensor used in the experiments

$\boldsymbol{\omega}_E(t)$ shall be explicitly determined resorting to the filtered measurements of $\mathbf{m}(t)$ and to the estimates of the auxiliary vector $\boldsymbol{x}_2(t)$. A stylized concept comprising the North-East-Down (NED) frames and vectorial quantities involved in this problem is depicted in Figure 1. A few additional steps are

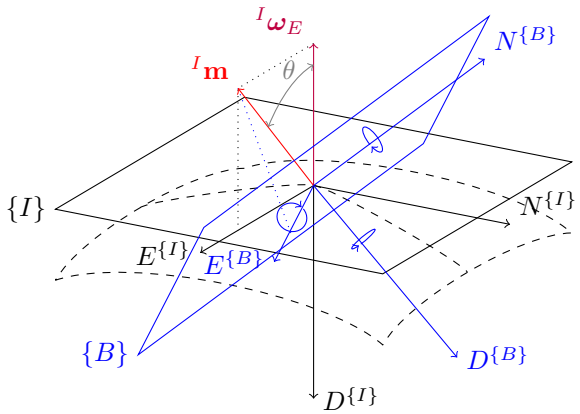

Figure 1: Visual conceptualization of the problem statement. Earth's curvature depicted as dashed lines.

required to write the linear differential equations associated with the system states. However, since these steps have already been thoroughly sketched in [15], they are herein omitted. Without further ado, consider the nominal continuous-time linear time-varying (CT-LTV) system

$$\begin{cases} \dot{\boldsymbol{x}}_1(t) = -\mathbf{S}[\boldsymbol{\omega}_m(t)]\boldsymbol{x}_1(t) + \boldsymbol{x}_2(t) \\ \dot{\boldsymbol{x}}_2(t) = A_{21}\boldsymbol{x}_1(t) - \mathbf{S}[\boldsymbol{\omega}_m(t) - A_{22}\mathbf{m}(t)]\boldsymbol{x}_2(t) \end{cases}, \tag{2}$$

where $A_{21} := \frac{\left({}^I\mathbf{m}^T\,{}^I\boldsymbol{\omega}_E\right)^2}{\|{}^I\mathbf{m}\|^2} - \left\|{}^I\boldsymbol{\omega}_E\right\|^2 \in \mathbb{R}$, and $A_{22} := \frac{\left({}^I\mathbf{m}^T\,{}^I\boldsymbol{\omega}_E\right)\left\|{}^I\boldsymbol{\omega}_E\times{}^I\mathbf{m}\right\|^2}{\|{}^I\mathbf{m}\times({}^I\boldsymbol{\omega}_E\times{}^I\mathbf{m})\|^2} \in \mathbb{R}$. Proceed to define the general system state vector as $\boldsymbol{x}(t) := [\boldsymbol{x}_1^T(t)\ \boldsymbol{x}_2^T(t)]^T \in \mathbb{R}^6$. Accordingly, the CT-LTV system in (2) can be written in a more compact form as

$$\dot{\boldsymbol{x}}(t) = \mathbf{A}(t)\boldsymbol{x}(t), \tag{3}$$

where $\mathbf{A}(t) = \begin{bmatrix} -\mathbf{S}[\boldsymbol{\omega}_m(t)] & \mathbf{I} \\ A_{21}\mathbf{I} & -\mathbf{S}[\boldsymbol{\omega}_m(t) - A_{22}\mathbf{m}(t)] \end{bmatrix} \in \mathbb{R}^{6\times 6}$. Notice that $\mathbf{A}(t)$ is not expressed in function of $\boldsymbol{x}(t)$; it evolves only according to measurements. Indeed, as convincingly argued in [20], all entries of matrix $\mathbf{A}(t)$ may just be considered as continuous bounded known functions of t, whereby an LTV system can be taken in place of the original nonlinear system. The limitations of this premise are in line with practical considerations, in particular in what concerns noise over measurements during the experiments. The objective now is to find an exact DT-LTV version of (3).

The following assumptions are considered throughout the remainder of the paper.

Assumption 1. (Geometric) *The constant inertial vectors $^I\boldsymbol{\omega}_E$ and $^I\mathbf{m}$ are non-collinear, i.e., $^I\boldsymbol{\omega}_E \times {}^I\mathbf{m} \neq \mathbf{0}$.*

Based on this assumption, let θ denote the angle between the two constant inertial vectors, such that $0 < \theta < \pi$, which consequently allows to write $A_{21} = -\sin^2(\theta)\|{}^I\boldsymbol{\omega}_E\|^2 < 0$ and $A_{22} = \|{}^I\boldsymbol{\omega}_E\|/\|{}^I\mathbf{m}\|\cos(\theta)$.

Assumption 2. (Practical) *The rate gyro measurements are bounded for all time.*

Assumption 3. (Computational) *The angular velocity $\boldsymbol{\omega}_m(t)$ and the vector $\mathbf{m}(t)$ remain constant between sampling instants.*

This last assumption bridges the gap of information between two consecutive sampling instants. It is suitable for this kind of application, where motions are relatively slow and sampling times are much faster in comparison.

B. Designing the cascade's first KF

Let $T_k \in \mathbb{R}$ denote the sampling time between consecutive instants t_k and t_{k+1}, i.e., $T_k = t_{k+1} - t_k > 0$. Bearing **Assumption 3** in mind, it is easy to compute the exact discrete-time solution of the differential equation (3), which allows to establish a relationship between the system state at time t_k, $\mathbf{x}_k$, and at time t_{k+1}, $\mathbf{x}_{k+1}$. On that account, the discrete-time solution of (3) evolves according to

$$\mathbf{x}_{k+1} = e^{\mathbf{A}_k T_k}\mathbf{x}_k, \tag{4}$$

where

$$\mathbf{A}_k = \begin{bmatrix} -\mathbf{S}[\boldsymbol{\omega}_{mk}] & \mathbf{I} \\ A_{21}\mathbf{I} & -\mathbf{S}[\boldsymbol{\omega}_{mk} - A_{22}\mathbf{m}_k] \end{bmatrix} \in \mathbb{R}^{6\times 6}. \tag{5}$$

Similarly to the continuous-time version, here one has $\mathbf{x}_k = [\mathbf{x}_{1k}^T\ \mathbf{x}_{2k}^T]^T$, with $\mathbf{x}_{1k} = \mathbf{m}_k$ and $\mathbf{x}_{2k} = \boldsymbol{\omega}_{Ek} \times \mathbf{m}_k$. Finally, $\boldsymbol{\omega}_{mk}$ corresponds to the measurement of the angular velocity taken at time t_k.

Solving the 6×6 matrix exponential in (4) is relatively simple and rather fast if one resorts, for instance, to the function `expm` from MATLAB. However, a closed-form expression would be a more elegant and, at the same time, more practical solution if one is interested in applying the proposed algorithm on low-end digital systems other than on arbitrarily fast and numerically precise computers equipped with MATLAB or with other powerful numerical computing environments. Hence, the matrix in (5) needs to be somehow reorganized in a more convenient and familiar arrangement in order to avoid computations involving the series expansion of the matrix exponential. Moreover, by achieving a closed-form solution for the expression in (4), one is indeed paving the way for a simpler and unequivocal observability analysis of the system.

Notice that, since $\mathbf{x}_{1k} = \mathbf{m}_k$, it must be $\mathbf{S}[\mathbf{m}_k]\mathbf{x}_{1k} = \mathbf{0}$. Therefore, without changing the nominal dynamics of the system, $\mathbf{A}_k$ can be rewritten as

$$\mathbf{A}_k = \begin{bmatrix} -\mathbf{S}[\boldsymbol{\omega}_{mk} - A_{22}\mathbf{m}_k] & \mathbf{I} \\ A_{21}\mathbf{I} & -\mathbf{S}[\boldsymbol{\omega}_{mk} - A_{22}\mathbf{m}_k] \end{bmatrix},$$

which, in turn, can be rewritten as the Kronecker direct sum of two matrices: one constant and one block diagonal. It follows that $\mathbf{A}_k = \bar{\mathbf{A}} \oplus \mathbf{D}_k = \bar{\mathbf{A}} \otimes \mathbf{I}_3 + \mathbf{I}_2 \otimes \mathbf{D}_k$, where

$$\bar{\mathbf{A}} = \begin{bmatrix} -1 & 1 \\ A_{21} & -1 \end{bmatrix} \in \mathbb{R}^{2\times 2},$$

and $\mathbf{D}_k = \mathbf{I} - \mathbf{S}[\boldsymbol{\omega}_{mk} - A_{22}\mathbf{m}_k] \in \mathbb{R}^{3\times3}$. Next, [21, Proposition 11.1.7] states that $e^{\mathbf{A}\oplus\mathbf{B}} = e^{\mathbf{A}} \otimes e^{\mathbf{B}}$, which allows to rewrite (4) as $\mathbf{x}_{k+1} = e^{T_k\bar{\mathbf{A}}} \otimes e^{T_k\mathbf{D}_k}\mathbf{x}_k$.

Recall now the well known Rodrigues' rotation formula for computing the exponential map, exp: $\mathfrak{s}o(3) \to SO(3)$, from skew-symmetric matrices to orthogonal matrices, given by

$$e^{\mathbf{S}[\mathbf{v}]} = \begin{cases} \mathbf{I} + \dfrac{\sin(\|\mathbf{v}\|)}{\|\mathbf{v}\|}\mathbf{S}[\mathbf{v}] + \dfrac{1-\cos(\|\mathbf{v}\|)}{\|\mathbf{v}\|^2}\mathbf{S}^2[\mathbf{v}], & \mathbf{v} \neq \mathbf{0} \\ \mathbf{I}, & \mathbf{v} = \mathbf{0} \end{cases} \tag{6}$$

for any vector $\mathbf{v} \in \mathbb{R}^3$. Then, and since matrix multiplications with the identity are commutative, it follows from (6) that

$$\begin{aligned} e^{T_k\mathbf{D}_k} &= e^{T_k\mathbf{I} - T_k\mathbf{S}[\boldsymbol{\omega}_{mk} - A_{22}\mathbf{m}_k]} = e^{T_k\mathbf{I}}e^{-T_k\mathbf{S}[\boldsymbol{\omega}_{mk} - A_{22}\mathbf{m}_k]} \\ &= e^{T_k}\left(\mathbf{I} - \frac{\sin\left(\|T_k\left(\boldsymbol{\omega}_{mk} - A_{22}\mathbf{m}_k\right)\|\right)}{\|\boldsymbol{\omega}_{mk} - A_{22}\mathbf{m}_k\|}\mathbf{S}[\boldsymbol{\omega}_{mk} - A_{22}\mathbf{m}_k]\right. \\ &\quad \left. + \frac{1-\cos\left(\|T_k\left(\boldsymbol{\omega}_{mk} - A_{22}\mathbf{m}_k\right)\|\right)}{\|\boldsymbol{\omega}_{mk} - A_{22}\mathbf{m}_k\|^2}\mathbf{S}^2[\boldsymbol{\omega}_{mk} - A_{22}\mathbf{m}_k]\right) \end{aligned} \tag{7}$$

if $\boldsymbol{\omega}_{mk} \neq A_{22}\mathbf{m}_k$, or $e^{T_k\mathbf{D}_k} = e^{T_k}\mathbf{I}$ if $\boldsymbol{\omega}_{mk} = A_{22}\mathbf{m}_k$. For ease of representation throughout the remainder of this paper, define $\boldsymbol{\psi}_k := \boldsymbol{\omega}_{mk} - A_{22}\mathbf{m}_k$. Therefore, the interesting result achieved in (7) expresses a rotation of magnitude $\|T_k\boldsymbol{\psi}_k\|$ around the unit rotation vector $-\boldsymbol{\psi}_k/\|\boldsymbol{\psi}_k\|$, followed by a scaling factor equal to e^{T_k}. Hence, equation (7) ought to be written in a more accessible composition, for example, as $e^{T_k\mathbf{D}_k} = e^{T_k}\mathbf{R}_k^*$, where $\mathbf{R}_k^*$ is a proper orthogonal rotation matrix, i.e., $\mathbf{R}_k^* \in SO(3)$, with $\mathbf{R}_k^* = \mathbf{I}$ if $\boldsymbol{\psi}_k = \mathbf{0}$, or

$$\mathbf{R}_k^* := \mathbf{I} - \frac{\sin(\|T_k\boldsymbol{\psi}_k\|)}{\|\boldsymbol{\psi}_k\|}\mathbf{S}[\boldsymbol{\psi}_k] + \frac{1-\cos(\|T_k\boldsymbol{\psi}_k\|)}{\|\boldsymbol{\psi}_k\|^2}\mathbf{S}^2[\boldsymbol{\psi}_k]$$

if $\boldsymbol{\psi}_k \neq \mathbf{0}$. Finally, compute the exponential of the 2×2 matrix $T_k\bar{\mathbf{A}}$, which, taking into account the fact that $A_{21} < 0$, as suggested by **Assumption 1**, is given by

$$e^{T_k\bar{\mathbf{A}}} = e^{-T_k}\Delta_k, \tag{8}$$

where

$$\Delta_k := \begin{bmatrix} \cos(\delta_k) & \frac{\sin(\delta_k)}{\sqrt{|A_{21}|}} \\ -\sqrt{|A_{21}|}\sin(\delta_k) & \cos(\delta_k) \end{bmatrix}, \quad \det(\Delta_k) = 1, \tag{9}$$

with $\delta_k = T_k\sqrt{|A_{21}|} > 0$. For further details, the reader is referred to [21, Corollary 11.3.3]. The inverse of (9), useful in the sequel, is simply given by

$$\Delta_k^{-1} = \begin{bmatrix} \cos(\delta_k) & -\frac{\sin(\delta_k)}{\sqrt{|A_{21}|}} \\ \sqrt{|A_{21}|}\sin(\delta_k) & \cos(\delta_k) \end{bmatrix}.$$

The previous buildup helps writing the propagation equation of the system state vector, whose term $\mathbf{x}_{1k} = \mathbf{m}_k$ corresponds to the single body-vector measurements as well. Thus, regarding $\mathbf{x}_{1k}$ as an output, one can complete the full definition of the auxiliary DT-LTV system by writing

$$\begin{cases} \mathbf{x}_{k+1} = \boldsymbol{\Phi}_k\mathbf{x}_k + \mathbf{w}_k \\ \mathbf{y}_k = \mathbf{C}\mathbf{x}_k + \mathbf{n}_k \end{cases}, \tag{10}$$

where

$$\boldsymbol{\Phi}_k = \Delta_k \otimes \mathbf{R}_k^* \in \mathbb{R}^{6\times6} \tag{11}$$

is the transition matrix that drives the system from t_k to t_{k+1}, $\mathbf{C} = [\mathbf{I}\ \mathbf{0}] \in \mathbb{R}^{3\times6}$ is the constant observations matrix that relates the output of the system to the system state, and $\mathbf{w}_k$ and $\mathbf{n}_k$ are the process and observations noise, both assumed white and to correspond to zero mean multivariate normal distributions with covariances $\mathbf{Q}_k$, and $\mathbf{N}_k$, respectively.

C. Observability Analysis

The following assumption is used throughout the remainder of this paper.

Assumption 4. (Practical) *The sampling rate T_k is bounded from above and from below. In particular, there exist positive constants $\epsilon_1, \epsilon_2 \in \mathbb{R}$ such that $\epsilon_1 < T_k < \epsilon_2$.*

The classic KF is the natural solution for the DT-LTV system (10). Through its implementation, the noise over measurements $\mathbf{m}_k$ is filtered, while, simultaneously, a vector that is closely related to the Earth's angular velocity is estimated. If the system is u.c.o., then the resulting error estimates are shown to be GES [22]. The following theorem encloses the first part of the main result of this work.

Theorem 1. *The DT-LTV system* (10) *is observable for all $k \geq k_0$. Moreover, given* **Assumption 4** *and assuming $\epsilon_2 << \pi/\sqrt{|A_{21}|}$, the system is also u.c.o., which means the estimates of a KF synthesized from* (10) *converge globally exponentially fast to the actual values.*

Proof. When considering the minimum interval of sampling times for observability, the observability matrix associated with the pair $(\boldsymbol{\Phi}_k, \mathbf{C})$, denoted by $\boldsymbol{\mathcal{O}}[k,k+2]$, is given by

$$\boldsymbol{\mathcal{O}}[k,k+2] = \begin{bmatrix} \mathbf{C} \\ \mathbf{C}\boldsymbol{\Phi}_k \end{bmatrix} = \begin{bmatrix} \mathbf{I} & \mathbf{0} \\ \cos(\delta_k)\mathbf{R}_k^* & \frac{\sin(\delta_k)}{\sqrt{|A_{21}|}}\mathbf{R}_k^* \end{bmatrix}. \tag{12}$$

First, note that $\mathbf{R}_k^*$ is always non-singular by definition. Then, according to **Assumptions 1** and **4**, it must be $\delta_k \neq 0$. Still, $\sin(\delta_k) = 0 \implies \delta_k = m\pi$, for $m \in \mathbb{N}_{>0}$, which means (12) is not full rank when $T_k = m\pi/\sqrt{|A_{21}|}$, for some $m \in \mathbb{N}_{>0}$, but, based on **Assumption 4**, $T_k < \epsilon_2 << \pi/\sqrt{|A_{21}|}$. Hence, under the conditions established above, the observability matrix $\boldsymbol{\mathcal{O}}[k,k+2]$ is always full rank, thus implying that the DT-LTV system (10) is observable for all $k \geq k_0$.

According to [22, Definition 7.153], the DT-LTV system (10) is u.c.o. if

$$\exists_{\substack{N>0 \\ \alpha>0 \\ \beta>0}}\ \forall_{k\geq k_0} \quad \alpha\mathbf{I} \leq \boldsymbol{\mathcal{J}}[k+N,k] \leq \beta\mathbf{I}, \tag{13}$$

with

$$\boldsymbol{\mathcal{J}}[k+N,k] = \sum_{i=k}^{k+N} \boldsymbol{\Xi}^T[i,k+N]\mathbf{C}^T\mathbf{C}\boldsymbol{\Xi}[i,k+N],$$

where, for $i \in [k, k+N]$, the term $\boldsymbol{\Xi}[k+N,i]$ corresponds to the transition matrix that drives the system from t_i to t_{k+N}, and is given by

$$\boldsymbol{\Xi}[k+N,i] = \begin{cases} \prod_{l=1}^{k+N-i} \boldsymbol{\Phi}_{k+N-l}, & i < k+N \\ \mathbf{I}, & i = k+N \end{cases}. \tag{14}$$

One of the properties of the transition matrix asserts that $\mathbf{\Xi}[i,k+N]=\mathbf{\Xi}[k+N,i]^{-1}$. Moreover, based on (11), one can write, making use of the mixed-product property of the Kronecker product,

$$\prod_{l=1}^{k+N-i}\mathbf{\Phi}_{k+N-l}=\left(\prod_{l=1}^{k+N-i}\Delta_{k+N-l}\right)\otimes\left(\prod_{l=1}^{k+N-i}\mathbf{R}^{*}_{k+N-l}\right).$$

Notice that both matrices in the previous Kronecker product are invertible. Therefore, for $i<k+N$, the inverse of (14) satisfies

$$\mathbf{\Xi}[i,k+N]=\left(\prod_{l=i}^{k+N-1}\Delta_l^{-1}\right)\otimes\left(\prod_{l=i}^{k+N-1}(\mathbf{R}^{*}_l)^{-1}\right), \quad (15)$$

where the invertible product property of the Kronecker product was employed. The inverse of a rotation matrix equals its transpose. Therefore, as the right side of (15) expresses a Kronecker product between a matrix of scaling factors and a rotation matrix, it can be simplified, for $i<k+N$, as $\mathbf{\Xi}[i,k+N]=\mathbf{F}_i\otimes\bar{\mathbf{R}}_i$. Specifically, from the result stated in (8), one has

$$\begin{aligned}\mathbf{F}_i&=\prod_{l=i}^{k+N-1}e^{-T_l}e^{-T_l\bar{\mathbf{A}}}=e^{-\tau_i}e^{-\tau_i\bar{\mathbf{A}}}\\&=\begin{bmatrix}\cos\left(\tau_i\sqrt{|A_{21}|}\right)&-\frac{\sin\left(\tau_i\sqrt{|A_{21}|}\right)}{\sqrt{|A_{21}|}}\\\sqrt{|A_{21}|}\sin\left(\tau_i\sqrt{|A_{21}|}\right)&\cos\left(\tau_i\sqrt{|A_{21}|}\right)\end{bmatrix},\end{aligned}$$

with $\tau_i:=\sum_{l=i}^{k+N-1}T_l>(k+N-i)\epsilon_1>0$. Regarding $\bar{\mathbf{R}}_i$, since only its properties are of interest in the remainder of the proof, it is not explicitly determined. Next, let there be a unit vector $\mathbf{c}=[\mathbf{c}_1^T\ \mathbf{c}_2^T]^T\in\mathbb{R}^6$, with $\mathbf{c}_1$,$\mathbf{c}_2\in\mathbb{R}^3$, and left and right multiply it with all terms in (13) to convert the matrix expression into an equivalent scalar one, resulting in

$$\alpha\leq\mathbf{c}^T\boldsymbol{\mathcal{J}}[k+N,k]\mathbf{c}=\|\mathbf{c}_1\|^2+\sum_{i=k}^{k+N-1}\left\|\mathbf{C}\left(\mathbf{F}_i\otimes\bar{\mathbf{R}}_i\right)\mathbf{c}\right\|^2\leq\beta. \quad (16)$$

Regarding the right inequality, the upper bound is always satisfied as all matrices involved are norm-bounded, and in particular

$$\begin{aligned}\sum_{i=k}^{k+N-1}\left\|\mathbf{C}\left(\mathbf{F}_i\otimes\bar{\mathbf{R}}_i\right)\mathbf{c}\right\|^2&\leq\sum_{i=k}^{k+N-1}\|\mathbf{C}\|^2\left\|\left(\mathbf{F}_i\otimes\bar{\mathbf{R}}_i\right)\right\|^2\|\mathbf{c}\|^2\\&\leq\sum_{i=k}^{k+N-1}\left\|\left(\mathbf{F}_i\otimes\bar{\mathbf{R}}_i\right)\right\|^2\\&=\sum_{i=k}^{k+N-1}\|\mathbf{F}_i\|^2=\sum_{i=k}^{k+N-1}\sigma^2_{max}(\mathbf{F_i})\\&\leq\sum_{i=k}^{k+N-1}\|\mathbf{F}_i\|_F^2.\end{aligned}$$

Since the squared Frobenius norm of matrix $\mathbf{F}_i$ is given by

$$\|\mathbf{F}_i\|_F^2=\mathrm{tr}\left(\mathbf{F}_i\mathbf{F}_i^T\right)=\frac{2|A_{21}|+\sin^2\left(\tau_i\sqrt{|A_{21}|}\right)(1-|A_{21}|)}{|A_{21}|},$$

it follows that $2\leq\|\mathbf{F}_i\|_F^2\leq(1+|A_{21}|)/|A_{21}|$, which allows to set $\beta=1+N(1+|A_{21}|)/|A_{21}|$ as a suitable upper bound. Notice that $\beta>>\epsilon_2$.

On the other hand, regarding the left inequality in (16), isolate the last two terms of the series under a new term denoted by Γ to obtain

$$\alpha\leq\Gamma+\sum_{i=k}^{k+N-2}\left\|\cos\left(\tau_i\sqrt{|A_{21}|}\right)\mathbf{c}_1-\frac{\sin\left(\tau_i\sqrt{|A_{21}|}\right)}{\sqrt{|A_{21}|}}\mathbf{c}_2\right\|^2,$$

with

$$\begin{aligned}\Gamma=&\|\mathbf{c}_1\|^2\\&+\left\|\cos\left(\tau_{k+N-1}\sqrt{|A_{21}|}\right)\mathbf{c}_1-\frac{\sin\left(\tau_{k+N-1}\sqrt{|A_{21}|}\right)}{\sqrt{|A_{21}|}}\mathbf{c}_2\right\|^2.\end{aligned}$$

The previous result can be rewritten in quadratic form as $\Gamma=\mathbf{c}^T\left(\Upsilon\otimes\mathbf{I}\right)\mathbf{c}$, with

$$\Upsilon:=\begin{bmatrix}1+\cos^2\left(\tau_{k+N-1}\sqrt{|A_{21}|}\right)&-\frac{\sin\left(2\tau_{k+N-1}\sqrt{|A_{21}|}\right)}{2\sqrt{|A_{21}|}}\\-\frac{\sin\left(2\tau_{k+N-1}\sqrt{|A_{21}|}\right)}{2\sqrt{|A_{21}|}}&\frac{\sin^2\left(\tau_{k+N-1}\sqrt{|A_{21}|}\right)}{|A_{21}|}\end{bmatrix}. \quad (17)$$

As $\tau_{k+N-1}=T_{k+N-1}$, then, in light of the statement of the theorem, $T_{k+N-1}\sqrt{|A_{21}|}<<\pi$, whereby Υ is a positive-definite symmetric matrix, with determinant given by $\sin^2(\tau_{k+N-1}\sqrt{|A_{21}|})/|A_{21}|>0$. Thus, it follows that $\Gamma\geq\lambda_{min}(\Upsilon)>0$, where $\lambda_{min}(\Upsilon)$ stands for the minimum eigenvalue of (17). Furthermore, $T_{k+N-1}\sqrt{|A_{21}|}<<\pi$ also validates the small angles approximation in (17), resulting in $\Upsilon\approx\begin{bmatrix}2&-T_{k+N-1}\\-T_{k+N-1}&T^2_{k+N-1}\end{bmatrix}$. Hence, $\lambda_{min}(\Upsilon)=T^2_{k+N-1}/2>\epsilon_1^2/2$. Therefore, by setting $\alpha=\epsilon_1^2/2$, and by finally noticing that $\alpha<\beta$, one concludes the proof. □

Remark 1. *In the statement of* **Theorem 1***, the upper bound ϵ_2 was set to be much smaller than $\pi/\sqrt{|A_{21}|}$. Contextually, when taking into account the speed of Earth's rotation, herein set according to the sidereal day, i.e., $\left\|{}^I\boldsymbol{\omega}_E\right\|=7.2921150\times10^{-5}$ rad/s, the value expressed by $\pi/\sqrt{|A_{21}|}$ would correspond to absurd and impractical sampling times. Therefore, claiming that $\epsilon_2<<\pi/\sqrt{|A_{21}|}$ does not, by any means, compromise the feasibility of the proposed solution.*

D. Cascade's first KF Implementation

Let $\hat{\mathbf{x}}_k=[\hat{\mathbf{x}}_{1k}^T\ \hat{\mathbf{x}}_{2k}^T]^T$ denote the state estimate at t_k, given by a KF applied to the auxiliary DT-LTV system (10).

Herein it is important to stress out that $\mathbf{S}[\mathbf{m}_k]\hat{\mathbf{x}}_{1k}$ is no longer identically zero, as there is nothing imposing the estimates of $\mathbf{m}_k$, expressed by $\hat{\mathbf{x}}_{1k}$, to be collinear with the corresponding measurements. This has to be carefully taken into account when tuning the KF's covariance matrix of the process noise.

According to [15], an estimate of the angular velocity of the Earth can be determined as

$$\hat{\boldsymbol{\omega}}_{Ek}=A_{22}\hat{\mathbf{x}}_{1k}+\frac{\hat{\mathbf{x}}_{1k}\times\hat{\mathbf{x}}_{2k}}{\|{}^I\mathbf{m}\|^2}. \quad (18)$$

Naturally, as both $\hat{\mathbf{x}}_{1k}$ and $\hat{\mathbf{x}}_{2k}$ have GES error dynamics, the estimates $\hat{\boldsymbol{\omega}}_{Ek}$ also converge exponentially fast to zero for any given initial condition.

This brings to an end the design of the first KF in the proposed cascade for attitude estimation. In the next section, a second KF will be derived to obtain an estimate of the rotation matrix $\mathbf{R}_k$, aided by the estimates (18).

III. Estimation of Rotation Matrix

The second KF in the cascade will resort to: i) the body angular velocity readings from the triaxial high-grade rate gyro, $\boldsymbol{\omega}_{mk}$; ii) the filtered measurements yielded by the first KF, $\hat{\mathbf{x}}_{1k}$; and, iii) the estimates of the Earth's angular velocity, $\hat{\boldsymbol{\omega}}_{Ek}$. Combining these three vector quantities under a second DT-LTV system, and further considering the state estimate vector $\hat{\mathbf{x}}_k$ as part of a new set of observations will allow to estimate the corresponding rotation matrix, whose entries will converge asymptotically to elements of $SO(3)$.

A. Discrete-time attitude KF design

As suggested in [15], start by considering a stacked column representation of the rotation matrix $\mathbf{R}(t)$, given by $\mathbf{z}(t) = \begin{bmatrix}\mathbf{r}_1^T(t) & \mathbf{r}_2^T(t) & \mathbf{r}_3^T(t)\end{bmatrix}^T \in \mathbb{R}^9$, where $\mathbf{R}(t) = \begin{bmatrix}\mathbf{r}_1(t) & \mathbf{r}_2(t) & \mathbf{r}_3(t)\end{bmatrix}^T \in \mathbb{R}^{3\times 3}$. In nominal terms, it follows that $\dot{\mathbf{z}}(t) = -\mathbf{S}_3[\boldsymbol{\omega}_m(t) - \boldsymbol{\omega}_E(t)]\mathbf{z}(t)$, where $\mathbf{S}_3[\mathbf{x}] := \text{diag}\left(\mathbf{S}[\mathbf{x}], \mathbf{S}[\mathbf{x}], \mathbf{S}[\mathbf{x}]\right)$. Similarly to what was described at the beginning of Section II-B, solving this differential equation is straightforward if bearing in mind all the assumptions established. Thus, based on (6), one obtains $\mathbf{z}_{k+1} = \bar{\mathbf{R}}_{3,k}\mathbf{z}_k$, where $\bar{\mathbf{R}}_{3,k} = e^{-T_k\mathbf{S}_3[\boldsymbol{\omega}_{mk}-\boldsymbol{\omega}_{Ek}]} = \text{diag}(\bar{\mathbf{R}}_{\mathbf{z},k}, \bar{\mathbf{R}}_{\mathbf{z},k}, \bar{\mathbf{R}}_{\mathbf{z},k})$, with

$$\bar{\mathbf{R}}_{\mathbf{z},k} = \mathbf{I} - \frac{\sin\left(\|T_k\left(\boldsymbol{\omega}_{mk} - \boldsymbol{\omega}_{Ek}\right)\|\right)}{\|\boldsymbol{\omega}_{mk} - \boldsymbol{\omega}_{Ek}\|}\mathbf{S}[\boldsymbol{\omega}_{mk} - \boldsymbol{\omega}_{Ek}] + \frac{1-\cos\left(\|T_k\left(\boldsymbol{\omega}_{mk}-\boldsymbol{\omega}_{Ek}\right)\|\right)}{\|\boldsymbol{\omega}_{mk} - \boldsymbol{\omega}_{Ek}\|^2}\mathbf{S}^2[\boldsymbol{\omega}_{mk}-\boldsymbol{\omega}_{Ek}]$$

for $\boldsymbol{\omega}_{mk} \neq \boldsymbol{\omega}_{Ek}$, or $\bar{\mathbf{R}}_{\mathbf{z},k} = \mathbf{I}$ for $\boldsymbol{\omega}_{mk} = \boldsymbol{\omega}_{Ek}$. Define now the (nominal) observations as $\mathbf{v}_k = \mathbf{C}_2\mathbf{z}_k$, where

$$\mathbf{v}_k = \begin{bmatrix}\mathbf{x}_{1k}^T & \mathbf{x}_{2k}^T & \left(\mathbf{x}_{1k} \times \mathbf{x}_{2k}\right)^T\end{bmatrix}^T \in \mathbb{R}^9$$

and $\mathbf{C}_2 = \begin{bmatrix} {}^I\mathbf{m}^T \\ \left({}^I\boldsymbol{\omega}_E \times {}^I\mathbf{m}\right)^T \\ \left({}^I\mathbf{m} \times \left({}^I\boldsymbol{\omega}_E \times {}^I\mathbf{m}\right)\right)^T \end{bmatrix} \otimes \mathbf{I} \in \mathbb{R}^{9\times 9}$. Hence, in the presence of sensor noise, the DT-LTV system for attitude estimation can be written as

$$\begin{cases} \mathbf{z}_{k+1} = \bar{\mathbf{R}}_{3,k}\mathbf{z}_k + \mathbf{w}_{\mathbf{z},k} \\ \mathbf{v}_k = \mathbf{C}_2\mathbf{z}_k + \mathbf{n}_{\mathbf{z},k} \end{cases}, \tag{19}$$

where $\mathbf{w}_{\mathbf{z},k} \sim \mathcal{N}(\mathbf{0}, \mathbf{Q}_{\mathbf{z},k})$ and $\mathbf{n}_{\mathbf{z},k} \sim \mathcal{N}(\mathbf{0}, \mathbf{N}_{\mathbf{z},k})$. Both matrices $\mathbf{Q}_{\mathbf{z},k}$ and $\mathbf{N}_{\mathbf{z},k}$ are positive definite, representing the covariances of the process and observations noises, respectively. Letting $\hat{\mathbf{z}}_k$ denote the estimate of $\mathbf{z}_k$, a KF follows once again as the natural solution for (19), with the nominal values $\mathbf{x}_{1k}$, $\mathbf{x}_{2k}$ and $\boldsymbol{\omega}_{Ek}$ being replaced by their estimates $\hat{\mathbf{x}}_{1k}$, $\hat{\mathbf{x}}_{2k}$ and $\hat{\boldsymbol{\omega}}_{Ek}$, respectively.

Remark 2. *Since the actual values of the dynamics matrix $\bar{\mathbf{R}}_{3,k}$ and of the output $\mathbf{v}_k$ are not available, one must resort to estimates of these quantities. But, since the rate of decay of their associated error dynamics was shown to be exponential, one may assume these estimates to be, in fact, nominal values subjected to perturbations that decay exponentially fast with time. Furthermore, if the nominal system is u.c.o., and if the state and the matrices of the system are bounded, then a KF is a suitable estimator, as it was shown in [23], on a continuous-time framework. However, these results are analogous to the discrete-time formulation, since they rely exclusively on Kalman filtering theory, including solutions of the Riccati matrix equation and observability gramians, which entails a direct correspondence between continuous- and discrete-time settings [24].*

Remark 3. *In this work, high-grade gyroscopes are assumed available. These devices are extremely precise inertial measurement units that display very low noise levels. Hence, the terms that result from time-correlation are much smaller compared to the remaining ones, which means that the approximation on the propagation of the covariances in the KF is negligible; in turn, the KF is not optimal but still convergent.*

The output $\hat{\mathbf{z}}_k$ of this KF corresponds to an estimate of the rotation matrix $\mathbf{R}_k$ with GES error dynamics. However, the resulting rotation matrix estimates, henceforward denoted by $\hat{\mathbf{R}}_k$, do not belong to $SO(3)$ as the KF ignores topological constructions. Nevertheless, $\hat{\mathbf{R}}_k$ can be projected on $SO(3)$ *a posteriori*, for instance, through the technique described in [25, Proposition 3.5], which stems from the Singular Value Decomposition. Defining $\hat{\mathbf{R}}_{e,k}$ as the projection of the estimated rotation matrix onto the manifold, it follows that

$$\hat{\mathbf{R}}_{e,k} = \hat{\mathbf{R}}_k\mathbf{U}\text{diag}\left(\frac{1}{\sqrt{\Lambda_1}}, \frac{1}{\sqrt{\Lambda_2}}, \frac{s}{\sqrt{\Lambda_3}}\right)\mathbf{U}^T, \tag{20}$$

such that $\hat{\mathbf{R}}_k^T\hat{\mathbf{R}}_k = \mathbf{U}^T\text{diag}(\Lambda_1,\Lambda_2,\Lambda_3)\mathbf{U}$ and $s = 1$ if $\det(\hat{\mathbf{R}}_k) > 0$ or, else, if $s = -1$, then $\det(\hat{\mathbf{R}}_k) < 0$.

In general, if all elements of the estimated rotation matrix $\hat{\mathbf{R}}_k$ are sufficiently close to elements of $SO(3)$, the projection operator (20) is an efficient technique. Otherwise, as it is the case when $\det(\hat{\mathbf{R}}_k) = 0$, one can always resort to an open loop integration on $SO(3)$ of the previous attitude estimate by computing $\hat{\mathbf{R}}_{e,k} = \hat{\mathbf{R}}_{e,k-1}e^{-T_k\mathbf{S}[\boldsymbol{\omega}_k - \hat{\boldsymbol{\omega}}_{E,k}]}$.

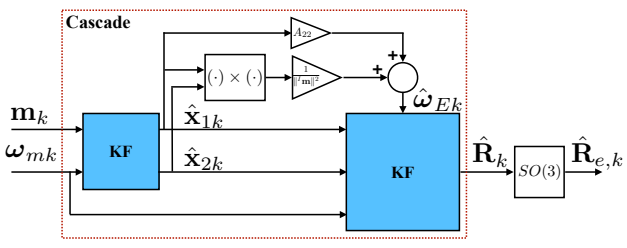

Figure 2: KF cascade enclosed in dashed red rectangle. The blocks for computing $\hat{\boldsymbol{\omega}}_{E,k}$ are arranged according to (18).

The final scheme of the KF cascade is depicted in Figure 2, where the $SO(3)$ block consists in a direct application of the

projection expressed by (20). This implementation requires a light computational workload.

B. Observability Analysis of Attitude Estimation Problem

This section encloses the second part of the main result of this work.

Theorem 2. *The DT-LTV system* (19) *is u.c.o., which means the KF estimates of the rotation matrix converge globally exponentially fast to the actual values.*

Proof. Following the same steps presented in II-C, according to [22, Definition 7.153], the DT-LTV system (19) is u.c.o. if

$$\exists_{\substack{\bar{N}>0\\ \bar{\alpha}>0\\ \bar{\beta}>0}} \forall_{k\geq k_0} \quad \bar{\alpha}\mathbf{I} \leq \boldsymbol{\mathcal{J}}_2[k+\bar{N},k] \leq \bar{\beta}\mathbf{I}, \tag{21}$$

with $\boldsymbol{\mathcal{J}}_2[k+\bar{N},k] = \sum_{i=k}^{k+\bar{N}} \boldsymbol{\Xi}_2^T[i,k+\bar{N}]\mathbf{C}_2^T\mathbf{C}_2\boldsymbol{\Xi}_2[i,k+\bar{N}]$, where, for $i \in [k,k+\bar{N}]$, the term $\boldsymbol{\Xi}_2[k+\bar{N},i]$ corresponds to the transition matrix, associated with pair $\left(\bar{\mathbf{R}}_{3,k},\mathbf{C}_2\right)$, that drives the system from t_i to $t_{k+\bar{N}}$, and is given by

$$\boldsymbol{\Xi}_2[k+\bar{N},i] = \begin{cases} \prod_{l=1}^{k+\bar{N}-i} \bar{\mathbf{R}}_{3,k+N-l}, & i < k+\bar{N} \\ \mathbf{I}, & i = k+\bar{N} \end{cases}.$$

Note that, for $i < k+\bar{N}$, the matrix $\boldsymbol{\Xi}_2[k+\bar{N},i]$ preserves the structure of $\bar{\mathbf{R}}_3$, a block diagonal of rotation matrices. Therefore, the inverse of $\boldsymbol{\Xi}_2[k+\bar{N},i]$ is also a block diagonal of rotation matrices. Furthermore, let there be a unit vector $\mathbf{d} = [\mathbf{d}_1^T\ \mathbf{d}_2^T\ \mathbf{d}_3^T]^T \in \mathbb{R}^9$, with $\mathbf{d}_1,\mathbf{d}_2,\mathbf{d}_3 \in \mathbb{R}^3$, and left and right multiply it with all terms in (21) to obtain

$$\bar{\alpha} \leq \sum_{i=k}^{k+\bar{N}} \left\|\mathbf{C}_2\boldsymbol{\Xi}_2[i,k+\bar{N}]\mathbf{d}\right\|^2 \leq \bar{\beta}. \tag{22}$$

Define $\bar{\mathbf{d}}_i := \boldsymbol{\Xi}_2[i,k+\bar{N}]\mathbf{d}$ as a unit vector that results from rotating $\mathbf{d}$, with $\bar{\mathbf{d}}_{k+\bar{N}} = \mathbf{d}$. Inequality (22) becomes

$$\bar{\alpha} \leq \sum_{i=k}^{k+\bar{N}} \left\|\mathbf{C}_2\bar{\mathbf{d}}_i\right\|^2 \leq \bar{\beta}. \tag{23}$$

An obvious upper bound is related to the spectral norm of $\mathbf{C}_2$, whereby one can set $\bar{\beta} = (\bar{N}+1)\|\mathbf{C}_2\|^2$. In regards to the lower bound, start by noticing that the summation consists entirely of non-negative terms. Moreover, based on **Assumption 1** and on the properties of the Kronecker product, the matrix $\mathbf{C}_2$ is shown to be full rank, as indicated below:

$$\text{rank}\left(\mathbf{C}_2\right) = \text{rank}\left(\begin{bmatrix} {}^I\mathbf{m}^T \\ \left({}^I\boldsymbol{\omega}_E \times {}^I\mathbf{m}\right)^T \\ \left({}^I\mathbf{m} \times \left({}^I\boldsymbol{\omega}_E \times {}^I\mathbf{m}\right)\right)^T \end{bmatrix}\right) \text{rank}(\mathbf{I}) = 9.$$

This means that the homogeneous system $\mathbf{C}_2\bar{\mathbf{d}}_i = \mathbf{0}$ is only verified by the trivial solution $\bar{\mathbf{d}}_i = \mathbf{0}$, but that contradicts the fact that $\|\bar{\mathbf{d}}_i\| = 1$ for all i. Therefore, a suitable lower bound is $\bar{\alpha} = \|\mathbf{C}_2\mathbf{d}\|^2$, which corresponds to the last term of the summation presented in (23), or, more specifically, to the square of the smallest singular value of $\mathbf{C}_2$. Specifically, by resorting to the singular value decomposition of $\mathbf{C}_2$, one easily deduces that the smallest singular value of $\mathbf{C}_2$ is given by $\min\left(\|{}^I\mathbf{m}\|^2,\ \|{}^I\boldsymbol{\omega}_E \times {}^I\mathbf{m}\|^2, \|{}^I\mathbf{m} \times \left({}^I\boldsymbol{\omega}_E \times {}^I\mathbf{m}\right)\|^2\right)$, thus concluding the proof. □

IV. Simulation Results

Consider a robotic platform describing a rotational motion while vector measurements of the gravitational field are collected by an accelerometer, and angular velocity readings are provided by a triaxial rate gyro. The attitude of the robotic platform evolves according to an angular velocity, which, in order to comply with **Assumption** 3, follows a discrete-time sequence given by $\boldsymbol{\omega}_k = \left[5\sin\left(\frac{2\pi}{60}k\right)\quad \sin\left(\frac{2\pi}{180}k\right)\quad -2\sin\left(\frac{2\pi}{300}k\right)\right]^T$ deg/s, for $k = 0,1,2,\ldots$. The sampling instants k correspond to instances when measurements are collected. Changes in other variables involved in the simulation are assumed to occur synchronized with these instants as well. In case data from different sensors were unsynchronized, i.e., low bandwidth measurements being fused with high bandwidth ones, complementary filtering techniques can be of assistance; for further details see [26].

To be coherent with the experimental setup in the next section, the location of the robotic platform's local inertial frame, in simulated environment, is considered to exist on the same geographical location as that of the real setup's own local inertial frame. Thus, select a NED geographical coordinate system as local inertial frame (see Figure 1), and choose the coordinates to be centered at a latitude of $\varphi = 38.777816°$ North, a longitude of $\lambda = 9.09757°$ West, and at sea level. As mentioned before in Section II-C, take into account the length of time known as sidereal day. The corresponding norm of the Earth's angular velocity is $\|{}^I\boldsymbol{\omega}_E\| = 7.2921159 \times 10^{-5}$ rad/s. Its vectorial representation in the NED frame is given by ${}^I\boldsymbol{\omega}_E = \|{}^I\boldsymbol{\omega}_E\|[\cos(\varphi)\ 0\ -\sin(\varphi)]^T$ rad/s. In light of the sea level and of the latitude indicated above, and according to the International Gravity Formula 1980, the components of the gravitational field are given by ${}^I\mathbf{m} = [0\ 0\ 9.80061]^T$ m/s^2. As such, ${}^I\boldsymbol{\omega}_E \times {}^I\mathbf{m} \neq \mathbf{0}$ ($\theta = 128.7778°$), which satisfies **Assumption** 1. The evolution of the rotation matrix follows by integrating the piecewise differentiable equation (1), starting from an initial attitude set to $\mathbf{R}_0 = \mathbf{I}$. In order to emulate the worst-case specifications of the FOG IMU KVH® 1775, with digital output, the rate gyro measurements are deemed corrupted by an angle random walk noise of $0.7°/\text{hr}/\sqrt{\text{Hz}}$, while a velocity random walk noise of $0.12\ \text{mg}/\sqrt{\text{Hz}}$ is considered for the accelerometer. The covariance matrices of the initial estimation error, process and observations noises of each KF were set as shown in Table I.

Since the measurements of the second KF correspond, in fact, to the estimates of the first one, the covariance matrix of the error concerning these estimates was feedforwarded to the second filter to act as covariance matrix of the observations noise. However, this only allows to obtain the covariance of the error regarding $\hat{\mathbf{x}}_1$ and $\hat{\mathbf{x}}_2$. Unfortunately, the covariance of the error associated with $\hat{\mathbf{x}}_1 \times \hat{\mathbf{x}}_2$ is not provided by the first filter, and its computation is not trivial. Therefore, through an empirical process, this covariance was set to $10^{-10}\mathbf{I}$, for which the best results were obtained. The initial estimates of

Table I: Covariance Matrices of the two KFs.

Covariance of the:	KF for $\hat{\boldsymbol{\omega}}_E$	KF for $\hat{\mathbf{R}}$
Initial error	diag($0.01\mathbf{I}$, $\mathbf{I}$)	$10^{-2}\times$diag($\mathbf{I}$, $\mathbf{I}$, $\mathbf{I}$);
Process noise	diag($10^{-9}\mathbf{I}$, $10^{-18}\mathbf{I}$)	$10^{-5}\times$diag($\mathbf{I}$, $\mathbf{I}$, $\mathbf{I}$)
Observations noise	$\left(\frac{0.3795}{1000} * 9.800611\right)^2\mathbf{I}$	*

the first KF were all set to zero, while the initial estimates of the second one were set to correspond to an initial attitude estimate equal to $\hat{\mathbf{R}}_{k=0} = \text{diag}(-1,1,-1)$, which is equivalent to a maximum angle error of 180 degrees. The sampling time in the simulations was set to a constant value of $T_k = 0.1$ s.

The plots with both the initial convergence and steady-state evolution of the estimation errors of $\hat{\mathbf{x}}_1$, $\hat{\mathbf{x}}_2$ and $\hat{\boldsymbol{\omega}}_E$ are displayed in Figures 3, 4 and 5, respectively. Henceforward, and in the same order, refer to $\tilde{\mathbf{x}}_1 := \mathbf{x}_1 - \hat{\mathbf{x}}_1$, $\tilde{\mathbf{x}}_2 := \mathbf{x}_2 - \hat{\mathbf{x}}_2$ and $\tilde{\boldsymbol{\omega}}_E = \boldsymbol{\omega}_E - \hat{\boldsymbol{\omega}}_E$ as the estimation errors of the first KF.

Overall, the cascade's first KF shows a very fast performance and, as opposed to the observer presented in [15], does not require a set of piecewise constant gains, which eases the burden of tuning gains. In steady-state, computed for $k \geq 4200$ ($t \geq 7$ min), the standard deviation of the Earth angular velocity error is $[0.0346\ 0.0184\ 0.023]^T$ deg/h in the NED frame, which is a good result when compared to the real sidereal angular velocity of 15.0411 deg/h. Likewise, for the same steady-state region, the standard deviations of the errors $\tilde{\mathbf{x}}_1$ and $\tilde{\mathbf{x}}_2$, in the NED frame, are $[0.028\ 0.0256\ 0.02505]^T$ mg and $[0.8985\ 0.8055\ 0.7120]^T$ mg/h, respectively, which compare well with the magnitude of the corresponding actual values, that is $\|\mathbf{x}_1\| = 1$ g and $\|\mathbf{x}_2\| = 1.6114$ g/h.

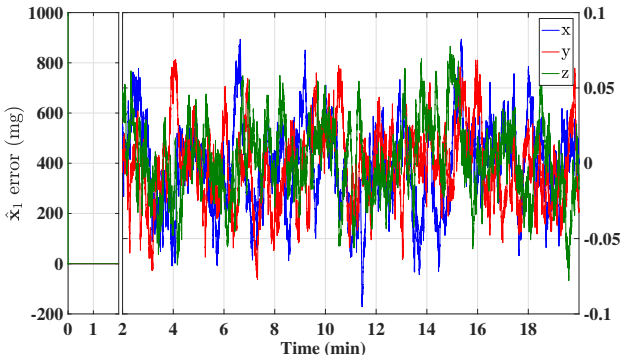

Figure 3: $\tilde{\mathbf{x}}_1$ - Estimation error of $\hat{\mathbf{x}}_1$.

Regarding the second filter, let $\tilde{\mathbf{z}} := \mathbf{z} - \hat{\mathbf{z}}$ be the error associated with the estimates of the rotation matrix. The plot of this error is shown in Figure 6, from where an evaluation is difficult to grasp. Instead, consider the axis-angle representation associated with the rotation matrix error, given by $\zeta_k = \frac{180}{\pi}\cos^{-1}\left(\frac{\text{tr}(\mathbf{R}_k^T\hat{\mathbf{R}}_{e,k})-1}{2}\right)$ deg, and observe the resulting plot, in Figure 7, for the evolution of the angle error. The initial rotation matrix estimate chosen before ensures that the angle error starts from its maximum deviation, 180 deg. The performance of this second filter is as fast as the first one in the cascade, exhibiting initial convergence times well below

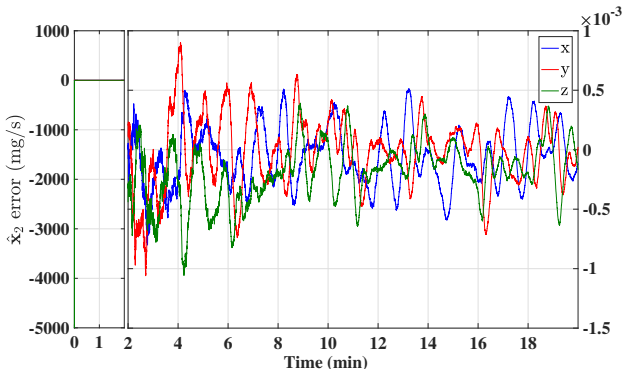

Figure 4: $\tilde{\mathbf{x}}_2$ - Estimation error of $\hat{\mathbf{x}}_2$.

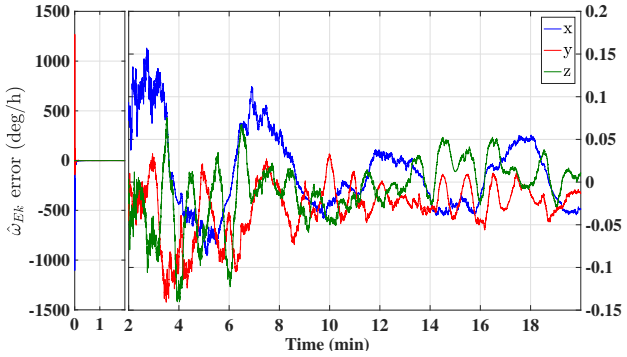

Figure 5: $\tilde{\boldsymbol{\omega}}_E$ - Estimation error of $\hat{\boldsymbol{\omega}}_E$.

the 1-min mark, as seen from both Figures 6 and 7. The mean angle error, computed for $k \geq 6000$ ($t \geq 10$ min), is 0.1638 degrees with a standard deviation of 0.0629 degrees, which deem the proposed solution a suitable choice for the problem of attitude estimation.

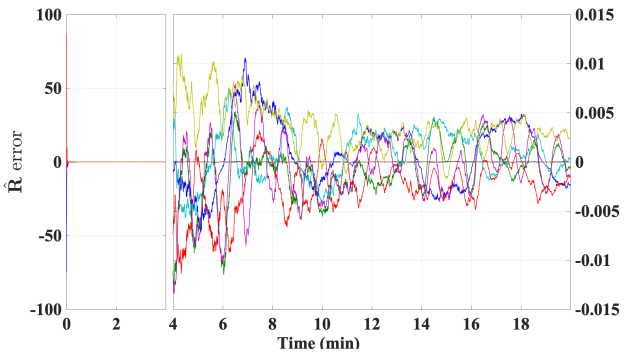

Figure 6: $\tilde{\mathbf{z}}$ - Estimation error of $\hat{\mathbf{z}}$.

V. Experimental Results

In order to validate the robustness of the proposed KF cascade, an experiment was conducted using a tri-axial high-grade FOG IMU KVH® 1775 mounted on an Ideal Aerosmith Model 2103HT Three-Axis Positioning and Motion Rate Table (MRT) System, which is designed to provide precise position, rate, and acceleration motion, for instance, for the development and/or production testing of IMUs. The ground-truth data from the MRT is characterized by a rate accuracy of $0.5\% \pm 0.0005$

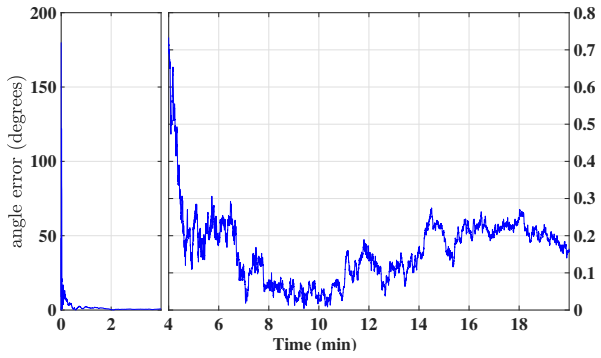

Figure 7: Angle representation error.

deg/s on its limited rotation axes (y and z) and $0.01\% \pm 0.0005$ deg/s on its unlimited rotation axis (x), and by a position accuracy of $30''$ on all axes. The final experimental setup is depicted in Figure 8.

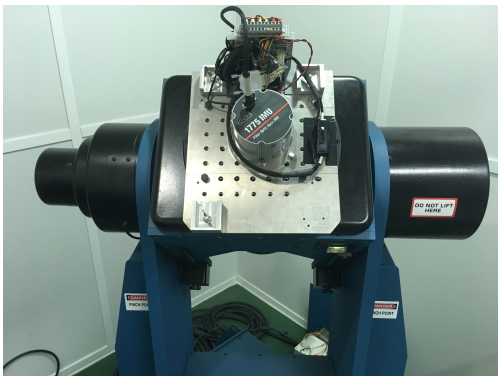

Figure 8: Experimental setup: FOG IMU KVH® 1775 mounted on a metal plate. The MRT's unlimited rotation axis is normal to the plate.

The FOG IMU provides tri-axial angular velocity, acceleration and magnetometer readings. The tri-axial magnetometer is unreliable because it is greatly affected, in this particular case, by the metallic structure of the MRT and magnetic fields induced by electrical currents on the motors, which cannot be compensated by calibration [27]. Therefore, we resort exclusively to accelerometer measurements, taking into consideration slow maneuvers in order to ensure that the approximation described in the beginning of Section II is valid. At room temperature, this FOG IMU's accelerometer is characterized by a velocity random walk of 0.12 mg$/\sqrt{\text{Hz}}$, the same used in the simulations. A calibration procedure was implemented beforehand that determined a matrix of constant scaling factors, a constant bias and a corresponding inertial vector (with respect to the MRT's own local NED inertial frame), for both the rate gyros and accelerometers. Data acquired from the MRT was sampled at 128 Hz, and later downsampled to 25 Hz to match the sampling frequency of the FOG IMU. The MRT is crucial in providing actual reference values for performance evaluation, while allowing for user inputs. Figure 9 shows the ground-truth data corresponding to the MRT's user-designed and user-programmed angular velocity, expressed in its reference frame.

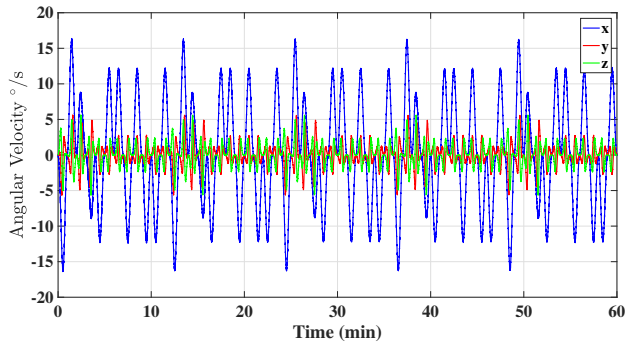

Figure 9: MRT angular velocity.

Table II: Experimental covariance Matrices of the two KFs.

Covariance of the:	KF for $\hat{\boldsymbol{\omega}}_E$	KF for $\hat{\mathbf{R}}$
Initial error	$\text{diag}(0.01\mathbf{I}, \mathbf{I})$	$10^{-2}\times\text{diag}(\mathbf{I}, \mathbf{I}, \mathbf{I})$;
Process noise	$\text{diag}(10^{-7}\mathbf{I}, 10^{-18}\mathbf{I})$	$10^{-10}\times\text{diag}(\mathbf{I}, \mathbf{I}, \mathbf{I})$
Observations noise	$\text{diag}(\begin{bmatrix}(9.695\times10^{-3})^2\\(3.047\times10^{-2})^2\\(2.902\times10^{-2})^2\end{bmatrix})$	*

The covariance matrices of the initial estimation error, process and observations noises of each KF were set according to Table II. Some values differ from those in Table I mainly due to the nature of the measurements. Furthermore, noises, which, in simulation, were assumed additive white Gaussian sequences, may not exactly share, in practice, the properties of normal distributions. In particular, the covariance of the observations noise was determined after a statistical analysis of the signals involved.

The plots with both the initial convergence and steady-state evolution of the estimation errors of $\hat{\mathbf{x}}_1$, $\hat{\mathbf{x}}_2$ and $\hat{\boldsymbol{\omega}}_E$ are displayed in Figures 10, 11 and 12, respectively. The magnitude of the steady-state error in Figure 12 compares well with that of Figure 5, which indicates a good performance in practice. Initial convergence times are almost unnoticeable, but that, compared to the simulated scenario, is somewhat expected in the sense that the sampling frequency in the experiments is 2.5 times faster than in simulation. Once again, in steady-state, this time computed for $k \geq 60000$ ($t \geq 40$ min), the standard deviation of the Earth angular velocity error is $[0.1203\ 0.2661\ 0.2139]^T$ deg/h in the NED frame. The computed standard deviations of the errors $\tilde{\mathbf{x}}_1$ and $\tilde{\mathbf{x}}_2$, also in the NED frame, are $[0.5044\ 1.3369\ 1.3948]^T$ mg and $[3.9732\ 3.3558\ 4.2108]^T$ mg/h, respectively, which compare very well with the magnitude of the corresponding real values, that is $\|\mathbf{x}_1\| = 1$ g $= 9.80061$ m/s^2 and $\|\mathbf{x}_2\| = 1.6114$ g/h. All these results are in line with the simulation outcomes achieved for the first KF in the cascade.

The plots with the evolutions of the rotation matrix error and the corresponding angle error are presented in Figures 13 and 14, respectively. As opposed to the simulation results, it takes approximately 15 minutes for both errors to reach steady-state. This might be related to the fact that, in the experiments, there exist vibrations caused by the MRT, leading to higher noise

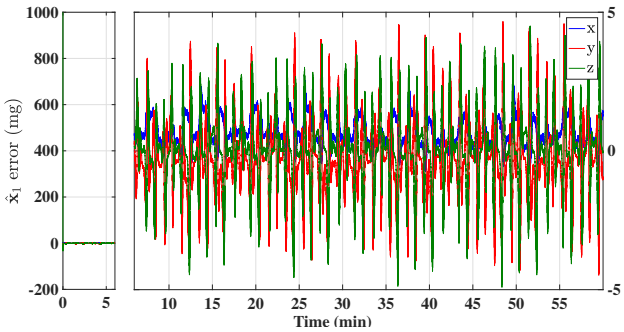

Figure 10: $\tilde{\mathbf{x}}_1$ - Experimental estimation error of $\hat{\mathbf{x}}_1$.

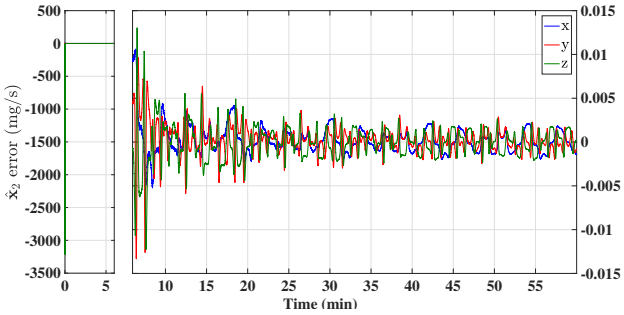

Figure 11: $\tilde{\mathbf{x}}_2$ - Experimental estimation error of $\hat{\mathbf{x}}_2$.

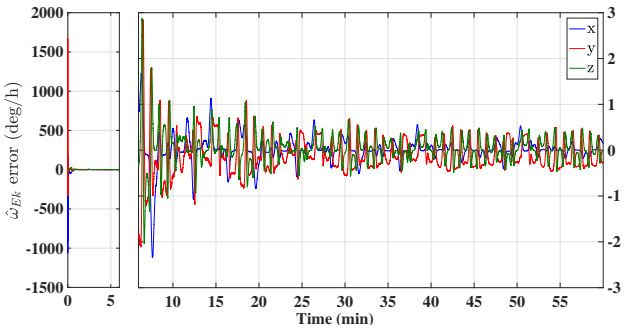

Figure 12: $\tilde{\boldsymbol{\omega}}_E$ - Experimental estimation error of $\hat{\boldsymbol{\omega}}_E$.

levels. Moreover, the acceleration may only be approximately constant when represented in inertial coordinates, which means that some term associated with an apparent force was not accounted for during the experiment. Finally, some mild model inaccuracies may have resulted from the calibration process. This however does not compromise the feasibility of the solution, as proven by its good convergence and steady-state accuracy. The results for the angle error are very good, with the mean and standard deviation, calculated also for ($t \geq 40$ min), equal to 0.4020 deg and 0.2207 deg, respectively.

VI. Conclusions

In this paper, a discrete-time attitude estimation solution featuring a cascade of two linear time-varying KFs was presented. The first filter in the cascade obtains an estimate of the Earth's angular velocity from a set of measurements that include angular velocity, provided by a triaxial high-grade rate gyro, and a body-vector whose inertial counterpart is constant. The output of the first KF, along with the same set

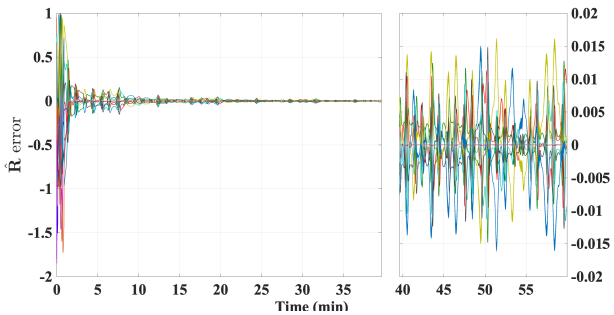

Figure 13: $\tilde{\mathbf{z}}$ - Experimental estimation error of $\hat{\mathbf{z}}$.

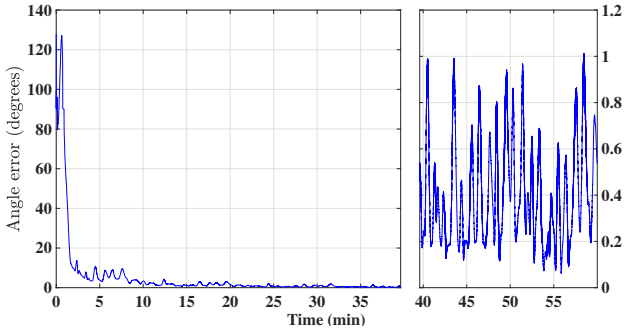

Figure 14: Experimental angle representation error.

of measurements, is feedforwarded to the second KF, which estimates a rotation matrix. This rotation, in spite of not belonging to $SO(3)$, has its entries converging exponentially fast to the manifold. The overall cascaded KF system was shown to be uniformly completely observable, in turn ensuring global exponential stability. Simulation and experimental results were presented that demonstrate the robustness of the proposed solution, which can be very useful for space and underwater applications, where high accuracy is required while simultaneously using high-grade rate gyros capable of sensing the Earth's rotation.

Acknowledgment

This work was supported by the Macao Science and Technology Development Fund under Grant FDCT/026/2017/A1, by the University of Macau, Macao, China, under Project MYRG2018-00198-FST and by the Portuguese Fundação para a Ciência e a Tecnologia (FCT) through Institute for Systems and Robotics (ISR), under Laboratory for Robotics and Engineering Systems (LARSyS) [UID/EEA/50009/2013] and through Institute for Mechanical Engineering (IDMEC), under Associated Laboratory for Energy, Transports and Aeronautics (LAETA) [UID/EMS/50022/2013] projects, and through the FCT project DECENTER [LISBOA-01-0145-FEDER-029605], funded by the Lisboa 2020 and PIDDAC programs.

References

[1] J. K. Deutschmann and I. Y. Bar-Itzhack. Evaluation of Attitude and Orbit Estimation Using Actual Earth Magnetic Field Data. *Journal of Guidance, Control, and Dynamics*, 24(3):616–623, May 2001.

[2] D. S. Laila, M. Lovera, and A. Astolfi. A discrete-time observer design for spacecraft attitude determination using an orthogonality-preserving algorithm. *Automatica*, 47(5):975 – 980, 2011.

[3] H. F. Grip, T. I. Fossen, T. A. Johansen, and A. Saberi. Attitude Estimation Using Biased Gyro and Vector Measurements With Time-Varying Reference Vectors. *IEEE Transactions on Automatic Control*, 57(5):1332–1338, May 2012.
[4] L. Chang, F. Zha, and F. Qin. Indirect Kalman Filtering Based Attitude Estimation for Low-Cost Attitude and Heading Reference Systems. *IEEE/ASME Transactions on Mechatronics*, 22(4):1850–1858, August 2017.
[5] H. Rehbinder and X. Hu. Drift-free attitude estimation for accelerated rigid bodies. *Automatica*, 40(4):653–659, April 2004.
[6] Y. Zhang, K. Song, J. Yi, P. Huang, Z. Duan, and Q. Zhao. Absolute Attitude Estimation of Rigid Body on Moving Platform Using Only Two Gyroscopes and Relative Measurements. *IEEE/ASME Transactions on Mechatronics*, 23(3):1350–1361, June 2018.
[7] G. Wahba. A Least Squares Estimate of Satellite Attitude. *SIAM Review*, 7(3):409–409, July 1965.
[8] E. J. Lefferts, F. L. Markley, and M. D. Shuster. Kalman Filtering for Spacecraft Attitude Estimation. *Journal of Guidance, Control, and Dynamics*, 5(5):417–429, September 1982.
[9] M. L. Psiaki, F. Martel, and P. K. Pal. Three-axis attitude determination via Kalman filtering of magnetometer data. *Journal of Guidance, Control, and Dynamics*, 13(3):506–514, May 1990.
[10] D. Mortari, F. L. Markley, and P. Singla. Optimal Linear Attitude Estimator. *Journal of Guidance, Control, and Dynamics*, 30(6):1619–1627, November 2007.
[11] M. Izadi, E. Samiei, A. K. Sanyal, and V. Kumar. Comparison of an attitude estimator based on the Lagrange-d'Alembert principle with some state-of-the-art filters. In *2015 IEEE International Conference on Robotics and Automation (ICRA)*. IEEE, May 2015.
[12] A. Barrau and S. Bonnabel. The Invariant Extended Kalman Filter as a Stable Observer. *IEEE Transactions on Automatic Control*, 62(4):1797–1812, April 2017.
[13] A. Barrau and S. Bonnabel. Intrinsic Filtering on Lie Groups With Applications to Attitude Estimation. *IEEE Transactions on Automatic Control*, 60(2):436–449, February 2015.
[14] J. Reis, P. Batista, P. Oliveira, and C. Silvestre. Nonlinear Observer on SO(3) for Attitude Estimation on Rotating Earth Using Single Vector Measurements. *IEEE Control Systems Letters*, 3(2):392–397, April 2019.
[15] P. Batista, C. Silvestre, and P. Oliveira. Globally exponentially stable attitude observer with Earth velocity estimation. *Asian Journal of Control*, March 2019.
[16] P. Batista, C. Silvestre, and P. Oliveira. Attitude observer on the special orthogonal group with Earth velocity estimation. *Systems & Control Letters*, 126:33–39, April 2019.
[17] A. Khosravian, T. J. Chin, I. Reid, and R. Mahony. A discrete-time attitude observer on SO(3) for vision and GPS fusion. In *Proc. IEEE Int. Conf. Robotics and Automation (ICRA)*, pages 5688–5695, May 2017.
[18] A. P. Vinod, A. D. Mahindrakar, S. Bandyopadhyay, and V. Muralidharan. A Deterministic Attitude Estimation Using a Single Vector Information and Rate Gyros. *IEEE/ASME Transactions on Mechatronics*, 20(5):2630–2636, October 2015.
[19] R. Mahony, T. Hamel, and J.-M. Pflimlin. Nonlinear Complementary Filters on the Special Orthogonal Group. *IEEE Transactions on Automatic Control*, 53(5):1203–1218, June 2008.
[20] P. Batista, C. Silvestre, and P. Oliveira. Sensor-Based Globally Asymptotically Stable Filters for Attitude Estimation: Analysis, Design, and Performance Evaluation. *IEEE Transactions on Automatic Control*, 57(8):2095–2100, August 2012.
[21] D.S. Bernstein. *Matrix mathematics: Theory, facts, and formulas with application to linear systems theory*, volume 41. Princeton University Press, 2009.
[22] A. H. Jazwinski. *Stochastic Processes and Filtering Theory*. Mathematics in Science and Engineering. Elsevier Science, 1970.
[23] D. Viegas, P. Batista, P. Oliveira, and C. Silvestre. On the stability of the continuous-time Kalman filter subject to exponentially decaying perturbations. *Systems & Control Letters*, 89:41 – 46, 2016.
[24] M. W. A. Smith and A. P. Roberts. An exact equivalence between the discrete- and continuous-time formulations of the Kalman filter. *Mathematics and Computers in Simulation*, 20(2):102–109, June 1978.
[25] M. Moakher. Means and Averaging in the Group of Rotations. *SIAM Journal on Matrix Analysis and Applications*, 24(1):1–16, 2002.
[26] R. Mahony, T. Hamel, and J.-M. Pflimlin. Complementary filter design on the special orthogonal group SO(3). In *Proceedings of the 44th IEEE Conference on Decision and Control*. IEEE, 2005.
[27] J. F. Vasconcelos, G. Elkaim, C. Silvestre, P. Oliveira, and B. Cardeira. Geometric Approach to Strapdown Magnetometer Calibration in Sensor Frame. *IEEE Transactions on Aerospace and Electronic Systems*, 47(2):1293–1306, April 2011.

Joel Reis received the M.Sc. degree in Aerospace Engineering, in 2013, from the Instituto Superior Técnico, Lisbon, Portugal. In 2014, he enrolled in the Electrical and Computer Engineering Ph.D. program at the University of Macau, where he is currently doing research at the Faculty of Science and Technology. His research interests include estimation theory based on underwater positioning and localization systems, and design of nonlinear attitude estimation algorithms.

Pedro Batista (SM IEEE) received the Licenciatura degree in Electrical and Computer Engineering in 2005 and the Ph.D. degree in 2010, both from Instituto Superior Técnico (IST), Lisbon, Portugal. From 2004 to 2006, he was a Monitor with the Department of Mathematics, IST. Since 2012 he is with the Department of Electrical and Computer Engineering of IST, he where he is currently Assistant Professor. His research interests include sensor-based navigation and control of autonomous vehicles. Dr. Batista has received the Diploma de Mérito twice during his graduation and his Ph.D. thesis was awarded the Best Robotics Ph.D. Thesis Award by the Portuguese Society of Robotics.

Paulo Oliveira (SM IEEE) received the "Licenciatura," M.S., and Ph.D. degrees in Electrical and Computer Engineering, and the Habilitation in Mechanical Engineering from Instituto Superior Tecnico (IST), Lisbon, Portugal, in 1991, 2002, and 2016, respectively. He is an Associate Professor in the Department of Mechanical Engineering of IST and Senior Researcher in the Associated Laboratory for Energy, Transports, and Aeronautics. His research interests are in the area of autonomous robotic vehicles with a focus on the fields of estimation, sensor fusion, navigation, positioning, and mechatronics. He is author or coauthor of more than 65 journal papers and 175 conference communications and participated in more than 30 European and Portuguese research projects, over the last 30 years.

Carlos Silvestre received the Licenciatura degree in Electrical Engineering from the Instituto Superior Tecnico (IST) of Lisbon, Portugal, in 1987 and the Master degree in Electrical Engineering and the Ph.D. degree in Control Science from the same school in 1991 and 2000, respectively. In 2011 he received the Habilitation in Electrical Engineering and Computers also from IST. Since 2000, he is with the Department of Electrical Engineering of the Instituto Superior Tecnico, where he is currently on leave. Since 2015 he is also with Faculty of Science and Technology of the University of Macau where he currently holds a Professor position with the Department of Electrical and Computers Engineering. His current research interests include linear and nonlinear control theory; hybrid systems; multi-agent control systems; networked control systems; inertial navigation systems and real time architectures for complex autonomous systems with application to unmanned air and underwater vehicles.